DESIGN AND ANALYSIS OF HIGHWAY TRANSPORTATION VIBRATION ISOLATION SYSTEM FOR HIGH PRECISION INSTRUMENT

Hongjun ZHANG[1,*], Lei WANG[2], Xiaohui WANG[3]

In response to the problem of reduced equipment accuracy and performance caused by road surface vibration, impact, and bumps during precision instrument road transportation, a road transportation isolation system was designed. The equivalent stiffness model and motion differential equation model of the isolator were established, and a six-legged isolation system was designed that met the load deformation and damping characteristics of the isolator according to experimental measurements. The isolation performance of the system was dynamically analyzed. The actual test results of road conditions indicate that the vibration isolation system has a good damping and suppression effect on ground random vibration loads greater than its first natural frequency, and has a good attenuation effect on random vibration loads greater than 6.67Hz in the main vibration direction. The precision instrument has a good damping effect during road transportation.

Keywords: precision instruments, vibration isolation systems, random vibration of highways, dynamic analysis

1. Introduction

Vibration isolation and vibration reduction are crucial to the road transportation of precision instruments [1]. In order to reduce the time limit for on-site assembly and commissioning of exact sciences instruments and the restrictions of on-site conditions, precision instruments generally need to be fully assembled and commissioned before transportation to ensure that they can be unpacked and used directly at the measurement and testing site, which poses a great challenge to the design of vibration isolation and vibration reduction systems in transportation engineering [2-3]. Precision instruments are prone to changes in key system parameters during vehicle transportation due to road vibrations, impacts, bumps, etc., resulting in inaccurate measurement results or inability to function properly, and even damaging precision instruments to cause significant economic losses [4-5]. Although transport vehicles can provide a certain degree of vibration reduction, they are far from meeting the transportation needs of precision instruments.

[1]* School of Mechanical and Electrical Engineering, Lingnan Normal University, China, e-mail: zhj118@yeah.net (corresponding author)
[2] School of Mechanical and Electrical Engineering, Lingnan Normal University, China
[3] School of Mechanical and Electrical Engineering, Lingnan Normal University, China

Therefore, considering the complex and variable road conditions, it is necessary to design the vibration reduction system for precision instrument equipment transportation [6], ensuring that its key parameters do not drift and the safety of the instrument equipment [7-8].

Ma et al. [9] proposed a new type of maglev Stewart vibration isolation platform for vibration isolation in the microgravity environment, which combines the quasi zero stiffness of the maglev actuator with the high mobility of the Stewart platform to eliminate the total disturbance in linear feedback, but is limited to static use. The parallel air spring isolation system (PAVS) has excellent isolation performance [10]. For precision instrument transportation under abnormal road and eccentric load conditions, Du et al. [11] proposed a nonlinear dynamic model of PAVS with equal height control strategy. This model has good dynamic isolation effect, but has complex structure and high-cost problems. Reference [12] designed a package of AST3 based on dynamic analysis for the transportation difficulties of precision optical telescope. This article focuses on the special vibration isolation requirements of a large precision instrument, which is composed of 20 mirror surfaces and has a total weight of 1460kg. The maximum diameter is 300 mm, the minimum mirror thickness ratio is 1:10, the diameter is large, the thickness is relatively thin, and it is a key precision and easily damaged part [13]. The transportation process requires optical components to not deviate, so the requirements for vibration isolation are very high in harsh road conditions [14].

This article first analyzes and tests the road conditions to provide reference for the design of vibration isolation systems. Then, an equivalent stiffness model and a motion differential equation model of the vibration isolator are established. A six-legged vibration isolation system is designed that meets the load deformation and damping characteristics of the vibration isolator measured through experiments. Finally, a dynamic analysis is conducted.

2. Road condition analysis and testing

To verify the vibration effect of the isolation system during actual transportation, road tests are conducted to ensure that the driving process and path are as close as possible to the actual transportation situation. There are three types of road sections: urban paved sections, rural paved sections, and rural unpaved sections. There are no emergency braking situations during driving. The speed variation range is 50~80 km/h, and the whole journey is in a state of uniform speed. There is no obvious acceleration or deceleration change on the speed bump and potholed road, and there are no other interference factors during the whole journey.

The three-dimensional acceleration sensor (KISTLER 8688A5) is used for real-time detection of the entire road condition, and is attached to the bottom of the transportation vehicle through epoxy adhesive. There is no sensor detachment or

movement during driving. The eight channels acquisition system (Dewesoft SIRIUSi-8xACC) is used to collect acceleration sensor data without interruption. The X-direction of the sensor is the direction of vehicle travel, the Z-direction is the direction perpendicular to the ground, and the Y-direction is the direction perpendicular to vehicle travel. The three follow the right-hand coordinate system rule. In order to better observe the actual situation of transportation vibration process, Fourier transform was performed on the real-time data of the acceleration sensor to analyze the vibration types appearing in the formal process from the perspectives of time domain and frequency domain. In combination with relevant standards such as GB/T4857 and GJB150.16A-2009 [15-16], a section of data information with obvious vibration was selected, and disturbance data in the key energy range (0-200Hz frequency range) was intercepted for plotting, as shown in Fig. 1.

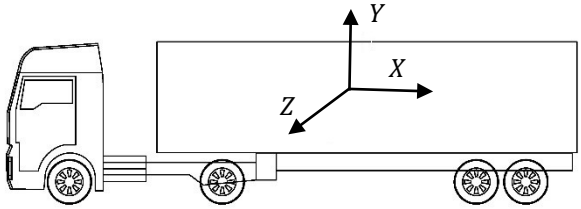

Fig.1. Schematic diagram of acceleration sensor direction in road condition test

From Fig. 2 to 4, it can be seen that the vibration amplitude in the Z-direction is the highest, and the maximum amplitude in the time domain frequency band can reach around 12g. The X-direction takes the second place, and the maximum amplitude in the time-domain frequency band is about 4g. The time domain situation in the Y- and X- directions is the same, with a maximum amplitude of about 4g. In the time domain frequency band, peaks appear in all three directions at the same time, and the result may be caused by the vibration isolation band on the driving path, while the vibration is relatively gentle in other time periods. From the perspective of frequency domain analysis, the energy bands with larger vibration amplitudes in the three directions are in the frequency range of 0-50Hz, and the Z-direction exhibits a peak amplitude of 0.32g at around 2Hz. The vibration forms in the X- and Y-directions are similar, with peaks of 0.13g and 0.14g at 45Hz and 35Hz, respectively.

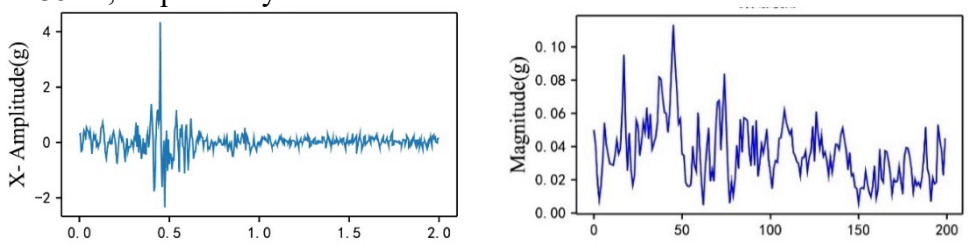

Fig. 2. X-direction road condition acquisition signal

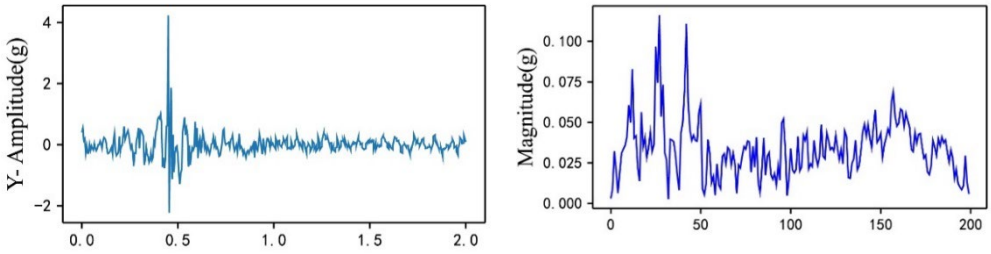

Fig. 3. *Y*-direction road condition acquisition signal

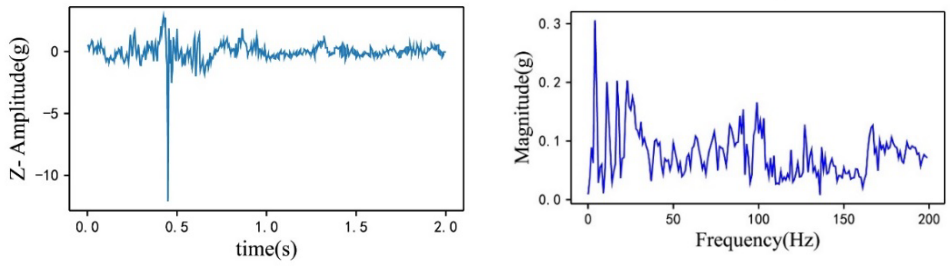

Fig. 4. *Z*-direction road condition acquisition signal

The above vibration patterns are in line with the relevant laws of highway vibration tests conducted by the Ministry of Transportation of China. The following can provide a reference for the design of the vibration isolation system, avoid the natural frequency of the vibration isolation system and the resonant frequency of highway vibration, and conduct peak staggering design to avoid the resonance of the packaging vibration isolation system, and minimize the damage of transportation vibration to optical instrument.

3. Vibration isolation design

3.1 Equivalent stiffness of vibration isolators

The elastic element undergoes bending deformation under radial tension (or pressure), and in calculation, the damper is considered as a uniformly supported beam at both ends. The shock absorber is rigidly connected to the base and payload, as shown in Fig.5. At displacement in y, the connection angle between the base and the shock absorber remains unchanged, but the payload has a small range of displacement.

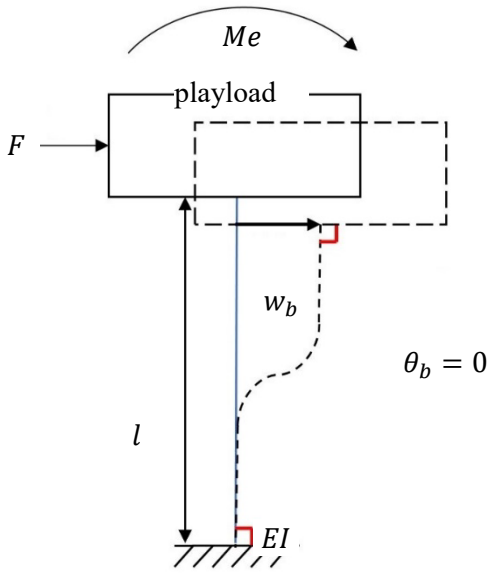

Fig. 5. Schematic diagram of equivalent beam bending deformation

E is the elastic modulus, I is the cross-sectional moment of inertia, w_b is the deflection, θ_b is the rotation angle. Using an equivalent beam, force F and moment M act on the fixed end of the damper. w_{b1} is the deflection under concentrated load, $\theta_{b1}$is the rotation angle under concentrated load, Me is the bending moment, and w_{b2} is the deflection under the bending moment, θ_{b2} is the rotation angle under bending moment. The full differential equation of Euler beams:

$$\frac{\partial^2}{\partial x^2}\left(EI\frac{\partial^2 w}{\partial x^2}\right) = q \tag{1}$$

where w represents displacement, and q represents the external force applied to the beam. Due to the fixed ends of the beam and the displacement of one fixed end, it is a statically indeterminate beam with:

$$\theta_b = \theta_{b_1} + \theta_{b_2} = 0 \tag{2}$$

therefore:

$$M_e = -\frac{Fl}{2} \tag{3}$$

the cross-sectional bending moment of the beam is:

$$M\,' = F(\frac{l}{2} - x) \tag{4}$$

therefore, the basic differential equation of a beam is:

$$\frac{\partial^2 w}{\partial x^2} = \frac{F(\frac{l}{2}-x)}{EI} \tag{5}$$

the solution of the equation is:

$$w = \frac{F(\frac{lx^2}{2} - \frac{x^3}{3})}{2EI} + C_1 + xC_2 \tag{7}$$

the boundary conditions are:

$$w(0) = 0, \frac{\partial w}{\partial x}\,|_{x=l} = 0 \tag{8}$$

From the boundary conditions, it can be concluded that$C_1 = 0$ and $C_2 = 0$, thus :

$$w(x) = \frac{F}{12EI}\,(3lx^2 - 2x^3\,) \tag{9}$$

when the mass block above the isolator deviates ($x = l$), the displacement of the end point is:

$$w_b = \frac{Fl^3}{12EI} \tag{10}$$

Therefore, the Bending stiffness of the vibration isolator k_h can be equivalent to:

$$k_h = \frac{F}{w_b} = \frac{12EI}{l^3} \tag{11}$$

3.2 Differential equations of motion

Usually, the micro vibrations generated by vehicle movement are transmitted from the spacing structure by connecting bolts [17], and the proposed vibration isolator is installed here. Fig.6 is a schematic diagram of a six-legged passive vibration isolation system. The system consists of an upper platform and its base, with a rigid mass block installed on the platform and a vertical height of l for the isolation unit. Assuming that the platform is a rigid body with a total mass of m=1460kg, the mass of the isolation system is much smaller than that of the upper platform and the overall mass block, so its mass size is not considered.

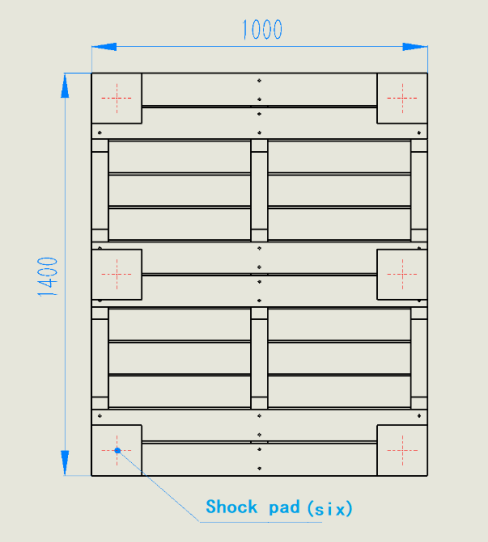

Fig. 6. Schematic diagram of the position distribution of the shock absorber in the shock absorption packaging box

Assuming that all isolators have stiffness coefficients k and damping coefficients c, the upper platform positions and attitudes x, y, and z represent the displacement of the upper platform in the X-, Y-, and Z-directions, respectively. A single degree of freedom equations of motion is used to discretize the continuous system, ignoring the influence of the small rotation angle of the mass block. All coordinate systems within the system follow the right-hand rule.

The system kinetic energy is as follows:

$$E_k = \frac{1}{2}m\left(\dot{x}^2 + \dot{y}^2 + \dot{z}^2\right) \tag{12}$$

The system potential energy is as follows:

$$V = 3\left(k_x x^2 + k_y y^2 + k_z z^2\right) = 3k_h(x^2 + y^2) + 3k_v z^2 \tag{13}$$

The Rayleigh loss function of the system is as follows:

$$R = 3\left(c_x \dot{x}^2 + c_y \dot{y}^2 + c_z \dot{z}^2\right) \tag{14}$$

The Lagrange equation is expressed as follows:

$$\frac{\mathrm{d}}{\mathrm{d}t}\left(\frac{\partial E_k}{\partial \dot{q}_i}\right) - \frac{\partial E_k}{\partial q_i} + \frac{\partial V}{\partial q_i} + \frac{\partial R}{\partial q_i} = Q_i \quad i = 1,2,\cdots,6 \tag{15}$$

By substituting equations 11-14 into equation 15, the motion differential equations of the 6-legged passive isolation system can be derived, expressed as follows:

$$m\ddot{x} + \frac{72EI}{l^3}x + c_x\dot{x} = A\sin(\omega t - \varphi) \tag{16a}$$

$$m\ddot{y} + \frac{72EI}{l^3}y + c_y\dot{y} = B\sin(\omega t - \varphi) \tag{16b}$$

$$m\ddot{z} + 6k_v z + c_z\dot{z} = C\sin(\omega t - \varphi) \tag{16c}$$

where,

$$A = X\left[\left(\frac{72EI}{l^3}\right)^2 + (c_x\omega)^2\right]^{\frac{1}{2}} \tag{17a}$$

$$B = Y\left[\left(\frac{72EI}{l^3}\right)^2 + \left(c_y\omega\right)^2\right]^{\frac{1}{2}} \tag{17b}$$

$$C = Z[36k_v^2 + (c_z\omega)^2]^{\frac{1}{2}} \tag{17c}$$

X、Y、Z represent the amplitude of the foundation during periodic motion, ω represents the excitation frequency during foundation vibration, φ represents phase, c_x, $c_y$and c_z represent system damping in each direction.

4. Performance analysis of vibration isolation schemes

The displacement transfer rate is the ratio of the amplitude of the response to the amplitude of the basic motion. According to equation 16a, the steady-state response $x(t)$ in the X-direction can be obtained, expressed as follows:

$$x(t)=\frac{X\sqrt{\left(\frac{12EI}{l^3}\right)^2+(c_x\omega)^2}}{\left[\left(\frac{12EI}{l^3}-m\omega^2\right)^2+(c_x\omega)^2\right]^{\frac{1}{2}}}sin(\omega t-\varphi) \tag{18}$$

According to the definition of displacement transfer rate, its manifestation is as follows:

$$T_d=\left[\frac{\left(\frac{12EI}{l^3}\right)^2+(c_x\omega)^2}{\left(\frac{12EI}{l^3}-m\omega^2\right)^2+(c_x\omega)^2}\right]^{\frac{1}{2}}=\left[\frac{1+(2\zeta_x r_x)^2}{\left(1-r_x^2\right)^2+(2\zeta_x r_x)^2}\right]^{\frac{1}{2}} \tag{19}$$

where, ζ_x represents the damping ratio of the isolator in the x direction, $r_x=\frac{\omega}{\omega_x}$ represents the frequency ratio in the x direction. $\omega_x=\sqrt{\frac{6k_h}{m}}=\sqrt{\frac{72EI}{ml^3}}$ represents the natural frequency of the system in the X-direction.

The acceleration transfer rate T is defined as the ratio of the amplitude of the acceleration response to the amplitude of the foundation. By taking the second derivative of the displacement response function and the basic displacement motion function separately, the corresponding acceleration function can be obtained, and thus the acceleration transfer rate can be obtained, which is in the same form as the displacement transfer rate function,

$$T=T_d=\left[\frac{1+(2\zeta_x r_x)^2}{\left(1-r_x^2\right)^2+(2\zeta_x r_x)^2}\right]^{\frac{1}{2}} \tag{20}$$

Firstly, the load deformation characteristics of a single isolator were measured using a testing machine, as shown in Fig.7, where the load was controlled by the displacement method. During the stretching and compression stages, the overall trend of load deformation shows a linear change. From this, it can be concluded that the axial stiffness of the isolator is about 200N/mm, and the axial natural circular frequency is ω_z =30Hz. The minimum section radius of the vibration isolator is 27mm, and the maximum section radius is 32mm, so the effective radius is 29.5mm, l=54mm. According to the equivalent beam model, the

bending stiffness of the vibration isolator is $k_h = 9 \times 10^4 N/mm$ and the natural angular frequency in the Oxy plane motion is $\omega_x = \omega_y = 606Hz$.

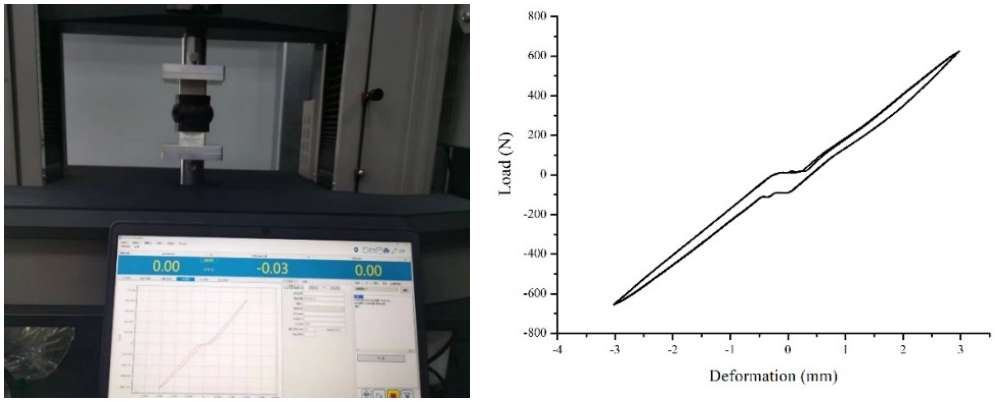

Fig. 7. Load deformation characteristics of a single isolator

Based on the hammer impact method to measure the damping of the isolator, FFT is used to convert the time-domain signal to the frequency domain, and the results are shown in Fig. 8. According to the half power method [18]:

$$\zeta = \frac{\omega_2 - \omega_1}{2\omega_n} \tag{21}$$

Among them, ζ is the damping ratio, ω_1 and ω_2 are the frequency corresponding to the half power point, ω_n is the fundamental frequency of the isolator. The damping ratios of the isolator in the X-, Y- and Z- directions are 0.1, 0.057, and 0.076, respectively.

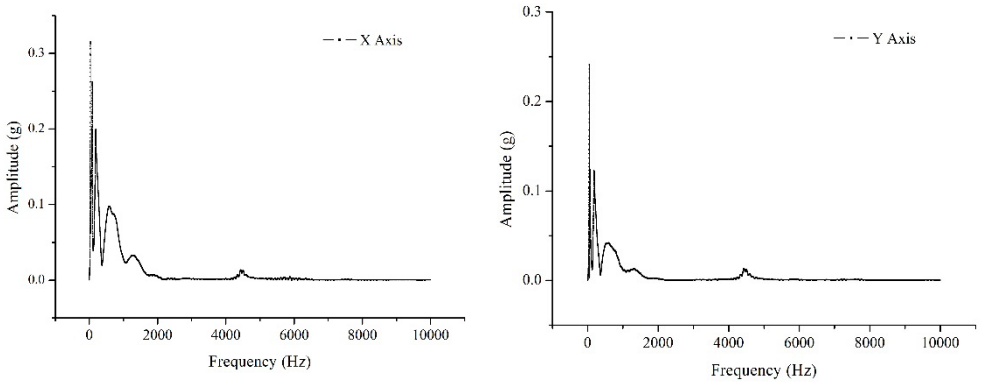

(a) X-direction (b) Y-direction

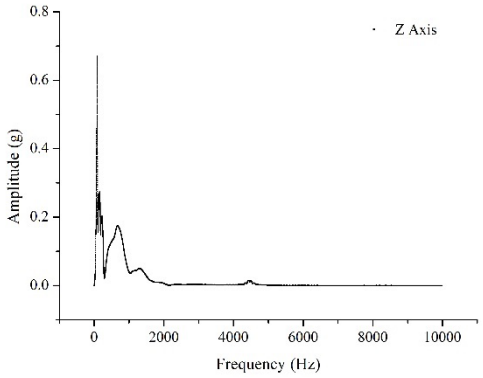

(c) Z-direction

Fig. 8. Frequency domain results of hammering method

Based on the above experimental results, by substituting the stiffness and damping ratio of the isolator into the acceleration transfer rate function, the transfer rate curve of the system can be drawn, as shown in Fig. 9.

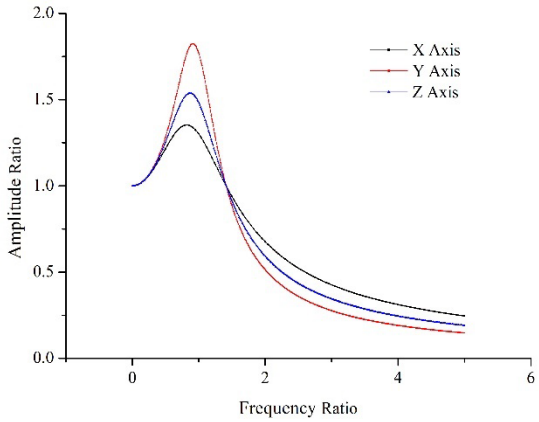

Fig.9. Acceleration transmission rate curve of hexapod isolation system

According to Fig. 9, when the frequency ratio is greater than $\sqrt{2}$ times, it will have a good vibration reduction effect. According to mathematical analysis, the natural circular frequency in the Z-direction is $\omega_2 = 30Hz$, according to the calculation formula $\omega = 2\pi f$ to calculate its natural frequencies, the results are $f_x = 96.5Hz$,$f_y = 96.5Hz$ and$f_z = 4.77Hz$ respectively.

According to the analysis of road conditions, peak excitation occurs at around $2Hz$ in the Z -direction, and at $45Hz$ and $35Hz$ in the X- and Y-directions, respectively. It is far from the natural frequency of the system, and the vibration energy will not be significantly amplified at this frequency point. The system generates significant vibration excitation in the Z-direction, which is the main vibration direction. According to vibration theory, when the frequency ratio is

greater than $\sqrt{2}$, the system achieves passive attenuation effect. That is, when the Z-direction excitation is greater than $6.69Hz$, vibration attenuation can be achieved. The higher the load frequency, the more obvious the vibration reduction effect. When the frequency ratio is 2 times, it can attenuate 60%, when it is 3 times, it can reach 70%, and when it is more than 3 times, it can be better than 80%. The results show that the design of the hexapod vibration isolation system has good vibration reduction effect.

6. Conclusions

In this article, the vibration isolation system of large by high precision optical instrument is studied. A vibration isolation system model was theoretically derived, and the vibration reduction performance was analyzed and evaluated based on the measured results of urban and rural road conditions. The results showed that the peak frequency of random vibration load under road conditions was far from the natural frequency of the system, and the vibration energy would not be significantly amplified at this frequency point. The system generates significant vibration excitation in the Z-direction, and this vibration isolation scheme can achieve vibration attenuation for random vibration loads greater than $6.69Hz$. The isolation effect becomes more pronounced as the load frequency increases. At the same time, the rationality and effectiveness of the vibration isolation scheme described in this article have been verified, which can provide reference for the vibration isolation design of other similar equipment.

REFERENCES

[1]. *X. L. Yang, H. T.Wu, B. Chen, et al,* "Dynamic modeling and decoupled control of a flexible Stewart platform for vibration isolation", Journal of Sound and Vibration, 439,2019, pp.398-412.

[2]. *H.K. Wen,X.F.Gong, P.H.Cui, et al,* "Double Layer Floating Raft Vibration Attenuation System for Antarctic Survey Telescope Transport" , Journal of Vibration,Measurement &. Diagnosis, **vol. 39**, **no. 6**, Dec. 2019, pp. 1291-1297+1365.

[3]. *D. Qu,X.D. Liu,G.T. Liu,Y.F. Bai,et al,* "Vibration isolation characteristics and control strategy of parallel air spring system for transportation under abnormal road and eccentric load conditions", Measurement & Control, **vol. 52(3-4)**, 2021, pp. 252-268.

[4]. *J.Y. Zhao, S.P. Kang, L.Z. Fan*,"Damping Device Used in Large-scale Precision Equipment Rapid Transporter", Journal of Mechanical Engineering, **vol. 53**, **no. 1**, Jan. 2017, pp. 93-100.

[5].*H.Zhang, Q.L.Wang, Z.W.Xu,et al,* "Vibration Isolation Design and Test of an Optical Measuring Platform for Vehicle Transportation", Journal of Changchun University of Science and Technology(Natural Science Edition), **vol. 44**, **no. 4**, Aug. 2021, pp. 7-12.

[6].*J.G.Su, M.H.Jiang,* Simulation and Test of Road Transit for the Vibration Damping Transportation Boxes. noise and vibration control, **vol. 35**, **no. 4**, Aug. 2015, pp. 35-37.

[7]. *L.Zhao, L.Tang, C.S.Xiang,* "Analysis of Damping Performance for Vibration Isolation System of Precision Instrument Transport Vehicles", Journal of Xihua University. Natural Science, **vol. 30**, **no. 4**, Jul. 2011, pp. 1-4.

[8]. *Z.L.Le,X.Q.Cui, B.Z.Gu,* "Vibration isolation system for transportation of main mirror of a large Antarctic telescope", Infrared and Laser Engineering, **vol. 49**, **no. 9**, Sept. 2020, pp. 274-282.
[9]. *H. Ma, W.C.Chi, C.H.Wang,et al,* "Design of a Maglev Stewart Platform for the Microgravity Vibration Isolation". Aerospace, **vol. 9**, **no. 514**, Sept. 2022, pp. 1-13.
[10]. *W.J.Bu, J.W. Cheng, L. Shi,* "Alignment Control Reconfigurability Analysis and Autonomous Control Methods of Air Spring Vibration Isolation System for High Power Density Main Engine (HPDME-ASVIS)". Applied Sciences, **vol. 12**, **no. 8211**, 2022.
[11]. *D. Qu,X.D. Liu,G.T. Liu,Y.F. Bai,et al,* "Analysis of vibration isolation performance of parallel air spring system for precision equipment transportation", Measurement & Control, **vol. 52(3-4)**, 2019, pp. 291-302.
[12]. *H.K. Wen, X.F. Gong, R. Zhang,* "The package cushioning design of the first AST3 and its dynamics analysis", International Society for Optics and Photonics,2012.
[13]. *E.K.Baines, S.Blomquist, J.H.Clark III,et al,* "Simultaneous Six-way Observations from the Navy Precision Optical Interferometer". The Astronomical Journal, **vol. 165**, **no. 2** ,2023.
[14]. *M. Jocelyn,* "Initialization Procedures for Discrete and Semi-Discrete Optimal Transport". Computer-Aided Design, **vol.115,** 2019, pp.13-22.
[15]. GB/T4857, Vibration test standards. Beijing: Standards Press of China, 2003.
[16]. GJB150.16A-2009, Environmental testing methods for military equipment laboratories - Vibration testing. Beijing: Standards Press of China,2009.
[17]. *T.B. Lan, Q.Ren, X. Liu,* "Design and application of impact limiter for a spent fuel transport cask", Nuclear Engineering and Design,2023,405.
[18]. *Z. Lozia, P.Zdanowicz,* Simulation assessment of the half-power bandwidth method in testing shock absorbers, Open Engineering, **vol. 11**,2020,pp.120-129.